Modelling the shearing behaviour of joints using an improved shear box genesis approach in particle flow code (2D) and its validation

Li H.[1,2,3], Deng J. H.[2], Yin J. H.[3], Zhu J. B.[4*]

[1] Sichuan University-The Hong Kong Polytechnic University Institute for Disaster Management and Reconstruction, Sichuan University, Chengdu, China
[2] State Key Laboratory of Hydraulics and Mountain River Engineering, Sichuan University, Chengdu, China
[3] Department of Civil and Environmental Engineering, The Hong Kong Polytechnic University, Hong Kong, China
[4] State Key Laboratory of Hydraulic Engineering Simulation and Safety, School of Civil Engineering, Tianjin University, Tianjin, China
* Corresponding author, Email: jbzhu@tju.edu.cn; Tel: +86 18522694463;

Abstract:

The smooth joint contact model has been used extensively to simulate the shear behaviour of joints in the numerical simulations with particle flow code. Results from existing studies have revealed that this model suffers from the particle interlocking problem taking place at the shear displacement greater than the minimum particle diameter. To solve this problem, the shear box genesis approach was proposed, by which particles in the upper and lower halves of a joint are generated separately, and the intended joint plane will be added as a common boundary. However, the shear box genesis approach is not a satisfactory solution to the interlocking problem yet. Three problems are usually encountered in practice: first, particles are still likely to move across the intended joint plane and cause the interlocking; second, the shear box genesis approach inevitably causes the periodic change in the contact number along the intended joint plane; third, it is difficult to incorporate the nonlinear closure behaviour of joints. Therefore, this paper aims to solve the shortcomings, and to apply the improvements to the simulation of joint shear behaviour. The interlocking problem was successfully solved by introducing the joint side checking method, and specifying the value of maximum allowed closure. The periodic stress fluctuation during shearing was eliminated by the non-unified ball generation method. The nonlinear closure behaviour of joints was captured by embedding the Barton-Bandis model. To verify the applicability of the improvements to rough joints, a series of numerical and experimental direct shear tests of rough joints were conducted. In general, good agreements were achieved between the numerical modelling results and laboratory measurements. This improved shear box genesis approach enhances the ability of the smooth joint contact model to simulate the shear behaviour of joints, and also has the ability to track the damage evolution during the joint shearing process.

Keywords: rock joint, particle flow code, shear box genesis method, direct shear test

1 Introduction

There exist numerous defects and discontinuities, e.g., joints, of different scales in rock masses (Wang et al. 2016; Zhu et al. 2018), and the stability and safety of rock engineering, e.g., slopes, foundations, tunnels, dams and underground spaces, are strongly dependent on the mechanical and deformational behaviour of rock joints. For example, the collapse of underground openings in rock masses is usually due to the shear sliding of rock joints (Deng et al. 2015). In the past few decades, many nonlinear shear models of rock joints have been proposed. These models have the attraction of a sound mathematical foundation, but turn out to be practically feasible for only certain types of joints (Kulhawy, 1975; Plesha, 1987; Leong and Randolph, 1992; Oh et al., 2015; Karakus et al. 2016). There is still a lack of knowledge on the shear mechanism of rock joints, involving the degradation of a single asperity and the interaction between asperities (Wang et al., 2016; Mehranpour and Kulatilake, 2016). One reason for this deficiency is the technical limitation of laboratory measurement. The other reason might be the challenge of testing repeatability, due to the heterogeneity of rock matrix and the irreproducibility of rock joints.

With the rapid advance of computer technology, many researchers have studied the shearing behaviour of joints numerically (Potyondy and Cundall, 2004; Oh, 2005; Vosiniakos, 2007; Karami and Stead, 2008; Ivars et al., 2011). The particle flow code (PFC), a discrete element method, has been widely used to simulate the mechanical behaviour of rock joints (Bahaaddini et al., 2016; Vallejos et al., 2016). In the PFC, intact rock material is usually modelled by a dense packing of rigid particles that are bonded together at their contact points. And joints are usually represented by weak contacts, at which particles are not bonded and more likely to be separated under shear or tensile loadings. Therefore, the damage in joint walls can be reflected by the breaking of contact bonds, and the motion of joint surfaces can be represented by the deformation at weak contacts (Cundall and Hart, 1992). This visualized representation of failure makes the PFC a very convenient tool to study the joint shearing deformation as well as investigate the crack propagation in joint asperities (Fakhimi and Villegas, 2007; Li

et al., 2016; Yang et al., 2015).

Nowadays, the newly developed smooth joint contact model (SJCM) has been increasingly adopted to simulate the mechanical behaviour of discontinuities, e.g., joints in rock masses (Yin and Zhao. 2016). In the SJCM, the "smooth joint" is regarded as a set of elastic springs distributed uniformly over a hypothetical cross-section. This section is centred at the contact point of two particles, and oriented parallel to the intended joint plane (Itasca Consulting Group Inc., 2016). With this model, two particles can slip past each other along the hypothetical cross-section, regardless of the rigid-particle assumption, as shown in Fig. 1. Thus, the applied slip force maintains parallel to the shear direction during the whole shearing process (Ivars, et al., 2011).

However, the SJCM still has a few shortcomings in successfully modelling the shear behaviour of rock joints. The most noticeable one is the so-called "local interlocking" problem. It was first found by Bahaaddini et al. (2013), and results from the inability of the PFC to update newly created contacts with the SJCM. A detailed description of the process of particle interlocking has been given by Bahaaddini et al. (2013) and Mehranpour and Kulatilake (2017), which including three steps: 1) with the increase in shear displacement, particles are easy to move across the intended joint plane, and penetrate into the opposite block; 2) the contacts around these particles are still the bond particle model, causing stress concentration and local interlocking; 3) shear and normal stress suddenly increase, causing unrealistic shear failure on joint surfaces, as shown in Fig. 2.

To solve this problem, Bahaaddini et al. (2013) proposed the shear box genesis (SBG) approach, by which particles in the upper and lower halves of a joint are generated separately, and the intended joint plane can be added as a common boundary. Fig. 3 shows the distribution of particles and contacts in the upper and lower halves of a planar joint generated with the SBG approach. Here, particles that lie on the opposite sides of the joint are far enough to avoid the particle-penetration problem. It should be admitted

that this approach improves significantly the ability of the SJCM to study the shear behaviour of joints. The real profile of joints can be explicitly reproduced, and the degradation of asperities during shearing can be investigated in terms of the shear and tensile microcracks (Bahaaddini, 2017).

However, the SBG approach has not been a satisfactory solution to the local interlocking problem yet. Three problems are usually encountered in practice. First, under relatively high normal stresses, particles are still likely to move across the intended joint plane and cause interlocking. Second, during the shear process, the SBG approach inevitably causes the periodic change in the contact number along the intended joint plane. Third, it is hard to incorporate the nonlinear closure/contact behaviour of joints.

Therefore, the aim of this paper is to solve the three shortcomings, and to simulate the shear behaviour of rough joints with the improved SBG approach. Core problems about these shortcomings were discussed firstly. The corresponding solutions were then proposed and validated based on the shear and compression tests of planar joints. To verify the applicability of the improvements to rough joints, numerical and experimental direct shear tests were conducted on two types of artificial saw-tooth joints and a natural rock joint. Comparisons between modelling results and laboratory measurements were carried out with emphasis on the shear strength, shear stiffness and shear mechanisms. The improvements in the SBG approach could enhance the capability of the smooth joint contact model to simulate the shear behaviour of joints and to track the damage evolution during the joint shearing process.

2. Three major shortcomings of the SBG approach

2.1 The local interlocking problem under high normal stress

As mentioned above, since the SBG approach only increases the geometrical distance between particles, it could not avoid the interlocking problem in some special cases, e.g., under high normal stresses. This issue was first posed by Mehranpour and

Kulatilake (2017), suggested to use the joint side checking approach to solve the stress-concentration problem under high normal stresses. This approach will be discussed in detail in Section 3.1. The advantage of the joint side checking approach is obvious. It does not make any modification in the cycle sequence, thus will not slow down the computing speed. However, like the bond remove method (Cundall, 2000), the joint side checking approach also suffers from an inherent micro-scale roughness, due to the uneven size, circular shape and random distribution of particles (Bahaaddini et al., 2013).

In fact, Fig. 2 is a good example of the local interlocking problem under high normal stresses. The normal stress applied was 7 MPa, which equals to 20% of the uniaxial compressive strength of joint walls. The values of the model parameters are listed in Table 1, which were calibrated by two planar mortar joints and five cylindrical mortar samples using a standard calibration procedure introduced by Bahaaddini et al. (2013). Specifically, the SJCM parameters were calibrated by normal compression tests and direct shear tests of planar mortar joints, which were composed of two cube mortar blocks with a nominal size of 100×100×100 mm^3 and a contact area of 100×100 mm^2. The parallel bond model parameters were calibrated by a series of uniaxial compression tests on cylindrical mortar samples, which had a diameter of 50 mm and a height of 100 mm. The uniaxial compressive strength, the Young's modulus and the Poisson's ratio of the mortar material were 34 MPa, 7.95 GPa and 0.21, respectively.

2.2 The periodic change of the contact number

Here, the contact number was defined as the number of active contacts between the upper and lower blocks. This periodic change is attributed to the approximately symmetrical distribution of particles along the intended joint plane, as shown in Fig.3, and aggravates the stress fluctuations during shearing. Fig. 4 illustrates the shear stress-shear displacement curve and contact number-shear displacement curve from the numerical direct shear test of a planar joint under the normal stress of 1 MPa. It is clear that shear stress fluctuates immediately after the change of the contact number. In this

test, the joint geometric model is identical to the one shown in Fig. 2. Shear force was directly measured at the joint plane rather than walls, equalling to the sum of the shear force at all contacts between the upper and lower blocks.

2.3 Incapability of incorporating the nonlinear closure behaviour of joints

It has been widely accepted that joint normal stiffness changes with the increase of normal displacement in joint compressive tests (Goodman, 1976; Bandis et al., 1983; Malama and Kulatilake, 2003). However, the normal stress-displacement relationship of a planar joint is almost linear, when the joint geometric model is built by the SBG approach. This problem results from the normal stiffness parameter used in the SJCM, i.e., sj_{k_n}, which is a constant by default (Itasca Consulting Group Inc., 2016). Fig. 5 compares the normal stress-normal displacement curves from the experimental and numerical closure/compression tests on a planar mortal joint. In the experimental test, displacement monitoring transducers were mounted directly on the mortar blocks as close to the joint as possible to directly capture the joint deformation process. In the PFC simulation, a 2D joint model was generated using the SBG approach. Compressive stress was applied by moving the top and bottom walls. Joint deformation was measured by the overlap between particles lying on both sides of the intended joint plane. The values of model parameters are listed in Table 1.

Mehranpour and Kulatilake (2017) solved this problem by embedding a liner stiffness-stress relationship into the SJCM. Although this linear function is feasible (Kulatilake, 2016) to solve this problem, its disadvantage is obvious. It is difficult to define a definite stress level, at which the joint reaches the maximum allowable closure. The concept of the maximum allowable closure of joints was introduced by Bandis et al. (1981), who affirmed that when the joint normal displacement reaches the maximum allowable closure (approximately 0.3 mm in Fig. 5), the normal stress and stiffness sharply increase and tend to become infinite.

3 Improvements of the SBG approach and validation

3.1 Employing the joint side checking method

To solve the local interlocking problem under high normal stresses, the joint side checking method was employed. The implementing procedure of the joint side checking method was suggested by Mehranpour and Kulatilake (2017). Before the shear test, particles located below and above the intended joint plane are marked as lower and upper particles, respectively. During the shearing, the contacts between these lower and upper particles are checked in each time step. If a non-smooth joint contact is created, the location of this contact would be found, and the type of it would be transformed into the SJCM automatically. This is a simple self-correction process, with which the newly created contacts between particles originally positioned on the opposite sides of the joint are guaranteed to be the SJCM.

3.2 Introducing the joint maximum allowed closure

Combining the joint side checking method with the SBG approach has not been a satisfactory solution to the interlocking problem yet. It still cannot prevent particles from moving across the intended joint plane. To solve this problem, we introduced the maximum allowed closure (δ_{max}), as a parameter of the SJCM, to reflect the joint compressive limit on displacement. This means the overlap between the particles lying on the opposite sides of the joint has a maximum value. If only this value is less than the smallest diameter of the particles, the particle-penetration problem can be effectively avoided. In addition, since joint compressive stiffness cannot exceed the compressive stiffness of rock blocks, it is assumed in the present study that, when the maximum allowable closure is reached, joint normal stiffness equals to the compressive stiffness in the particle bond model.

3.3 Adopting the non-unified ball generation method

To eliminate the periodic stress fluctuation during shearing, we proposed the non-unified ball generation method, which adopts a more flexible pattern of particle generation than the traditional SBG approach. The core idea of this method is that

particles in the upper and lower blocks are of different size ranges. This method could break the symmetric arrangement of particles along the intended joint plane, thereby has the ability to alleviate the periodic change in the contact number. Fig. 6 shows an example of joint geometric model built by the non-unified ball generation method. It was found that the ratio of the average ball radii in the upper and lower blocks needs to be greater than 2.3, otherwise, a considerable stress fluctuation would be observed. This empirical value was obtained from a series of numerical direct shear tests on planar joins. The values of the model parameters were the same as those listed in Table 1.

3.4 Embedding the Barton-Bandis model

To capture the nonlinear compressive behaviour of joints, the Barton-Bandis model, i.e., BB model (Bandis et al., 1983), was embedded into the SJCM. An additional hyperbolic model is thus available in the SJCM for capturing the nonlinear stress-displacement relationship of joints. The normal stress-normal displacement relationship of joints satisfies:

$$\sigma_n = \frac{k_{ini}\delta}{1-\frac{\delta}{\delta_{\lim}}} \qquad (1)$$

Joint normal stiffness is given by

$$k_n = \frac{k_{ini}}{\left(1-\frac{\delta}{\delta_{\lim}}\right)^2} \qquad (2)$$

or

$$k_n = k_{ini}\left(1-\frac{\sigma_n}{k_{ini}\delta_{\lim}+\sigma_n}\right)^{-2} \qquad (3)$$

where k_n is the normal stiffness of joints, σ_n is the normal stress, δ is the normal displacement of joints, k_{ini} is the initial normal stiffness, and δ_{lim} is the compression displacement limit.

There is a slight difference between the maximum allowable closure (δ_{max}) and the

compression displacement limit (δ_{lim}). The former is the real maximum closure of joints measured in laboratory tests (e.g., 0.3 mm in Fig. 5), while the latter is a mathematic parameter in the BB model, which determines the domain of the hyperbolic function. Therefore, in practice, the values of these two parameters might be different.

3.5 Validation of the improved SBG approach

Direct shear tests

A series of numerical and experimental direct shear tests of planar mortar joints were carried out to validate the improved SBG approach. In experimental tests, the mortar joints were tested under constant normal stress conditions. The nominal size of the joints was 100×100×100 mm^3 with a contact area of 100×100 mm^2. Shear rates applied were all less than 0.01 mm/s. Normal stresses applied were 3 MPa, 5 MPa and 7 MPa, respectively. In numerical simulations, 2D joint profile models, with the nominal size of 100×50 mm^2 (as shown in Fig. 6), were built and tested under the same boundary conditions as the experimental tests. A smaller geometric model was built in numerical tests to reduce the number of particles and thus to save storage and computing time. The values of the model parameters are listed in Table 2. Table 3 compares the testing results from experimental and numerical uniaxial compression tests on intact mortar cylinders, which were used for parameter calibrations. Fig. 7 compares shear stress-shear displacement curves from numerical and experimental direct shear tests on the planar joints. It could be seen that numerical predictions agree well with laboratory testing results with respect to shear strength and shear stiffness. As expected, there is no sharp increase in shear stress, and the fluctuation of shear stress was acceptable in the numerical simulations. Therefore, the applicability of the joint side checking method and the non-unified ball generation method was successfully validated. It should be admitted that stress distributions in the numerical and experimental tests could be different, due to the different model size. However, this influence seems negligible to the stress-displacement curve.

Joint compressive tests

The numerical compression test mentioned in Section 2.3, was re-conducted employing the improved SBG approach. Similar to the joint specimens used in the shear tests, a 2D planar joint profile model with a nominal size of 100×50 mm^2 was built and tested under unconfined conditions. Values of the particle bond model parameters are listed in Table 2. Values of the SJCM parameters are listed in Table 4. Fig. 8 compares normal stress-normal displacement curves from the numerical and experimental tests. Good agreement was achieved between the numerical and experimental testing results. A nonlinear stress-displacement curve and a clear compressive limit on displacement were observed in the numerical compression test.

In fact, a factitious change of normal stiffness at the maximum allowable closure of joints could induce obvious stress fluctuations. This problem can be adequately solved when the shear/compression velocity decreases to a value of 1 mm/s or less, provided that the local damping value is equal to 0.7.

4 Steps for the use of the improved SBG approach

With the improved SBG approach, the smooth joint contact model becomes an effective tool for reproducing or predicting the mechanical behaviour of planar joints. In general, the following six steps were employed (valid for PFC 5.0 or newer):

1) *Building the geometric model*: Upper and lower blocks were generated by frictionless walls. 2D joint surfaces were digitalized and generated by a series of nodes.

2) *Assembling the particles:* Particles were assembled with different size ranges in upper and lower blocks. The ratio of average particle radii in the upper and lower blocks should be larger than 2.3.

3) *Adjusting the internal stress:* The number of floating balls (particles with less than three contacts) was reduced to 0.1% of the total particle number. The magnitude of internal locked-in stress was adjusted to reach an isotropic stress at 1% of the uniaxial compressive strength of joint walls.

4) *Installing the contact bonds:* The parallel bond model was assigned to the contacts providing the presentation of rock materials. The corresponding parameters were

calibrated through the uniaxial compression test of intact rock materials.

5) *Installing the SJCM:* The SJCM was installed at the contacts between the particles that originally lie on the opposite sides of the intended joint plane. The parameters in the BB model were calibrated by the compression/closure test of planar joints. The shear stiffness and friction coefficient were calibrated by the direct shear test of planar joints.

6) *Applying the normal and shear stresses:* Normal stress was applied by a servo-controlled wall. Shear stress was applied by lateral walls bonded together with sample surfaces. At each time step, newly created contacts between the particles originally positioned on the opposite sides of the joint were checked and assigned with the SJCM by the joint side checking method.

5 Application in modelling the shear behaviour of rough joints

To check the applicability of the improved SBG approach to rough joints, numerical and experimental direct shear tests of artificial and natural rough joints were carried out.

5.1 Direct shear tests of artificial rough joints with regular asperities

In laboratory tests, three mortar joints with saw-tooth asperities were sheared under constant normal load conditions. The dip angle of each single asperity is 20°. The wave/base length of each single asperity is 10 mm. Fig. 9 shows the profile of a joint specimen with regular asperities. The nominal size was 100×100×100 mm^3 with the contact area of 100×100 mm^2. Shear rates applied were less than 0.01 mm/s. Normal stresses applied were 1 MPa, 3 MPa and 5 MPa, respectively. In numerical tests, 2D joint profile models with the nominal size of 100×50 mm^2 were also tested under constant normal load conditions. Similar to the experimental tests, the upper block is free to move only in the vertical direction, and the lower block is free to move only in the horizontal direction. Parameter values used in the particle bond model and the improved SJCM are listed in Tables 2 and 4, respectively. Here, joint shear stiffness in the SJCM is 8.9 GPa/m instead of 0 GPa/m. Fig. 10 compares the shear stress-shear displacement curves from the experimental and numerical direct shear tests. It could be

seen that the shear strength and shear stiffness obtained from the numerical tests are in good agreement with the laboratory measurements.

Shear damage/failure patterns observed in the numerical direct shear tests are shown in Fig. 11. Four types of shearing mechanisms were observed in our tests: frictional sliding, surface wearing (obvious scraping), asperity shearing, and crushing (breaking into pieces). Specifically, under the normal stress of 1 MPa, shearing took place in the form of frictional sliding (Fig. 11a). Asperities slid along their surfaces, and only a limited number of cracks were formed during shearing. Under the normal stress of 3 MPa, surface wearing was observed (Fig. 11b). Cracks were formed mainly on the surface of asperities and did not propagate into joint walls. Under the normal stress of 5 MPa, asperities were sheared off and crushed (Fig. 11c). Cracks propagated into asperities, causing macro-fractures. This macro-scale failure of asperities can be clearly observed in the corresponding experimental test, as shown in Fig. 9b.

5.2 Direct shear tests of artificial rough joints with irregular asperities

Numerical and experimental direct shear tests of mortar joints with irregular asperities (i.e., irregular joints) were also conducted. Fig. 12 shows the geometric morphology of an irregular joint. Asperities with different dip angles (10°, 20° and 30°) were orderly placed to bring convenience for observing interactions between asperities. The nominal size of the joints was also 100×100×100 mm^3 with a contact area of 100×100 mm^2. 2D joint geometric models have a nominal size of 100×50 mm^2 in numerical tests. Normal stresses applied in numerical and experimental tests were exactly the same, varying among 1 MPa, 3 MPa and 5 MPa. Fig. 13 compares the testing results from the numerical and experimental direct shear tests. The agreement is good with respect to shear strength and shear stiffness. The typic shearing failure process observed in the numerical direct shear tests is shown in Fig. 14. As the shear displacement increased, frictional sliding first occurred on the steepest asperities (Fig. 14a and b). When the steepest asperities were sheared off, frictional sliding and wearing occurred on less steep asperities, causing non-uniform shear failure on the joint surface (Fig. 14b and c).

Load transfer between asperities was clearly illustrated by the force network/chain. Before the shear strength was reached, there was a gradual load-transfer process from the less steep asperities to the steepest asperities. Afterward, most shear loads were transferred back to the gentler ones.

5.3 A direct shear test of a natural rough joint

The numerical direct shear test was conducted on a mated granite joint. Testing results were then compared with the laboratory measurements obtained under the same testing condition. The geometric morphology of the joint is shown in Fig. 15a. The scanned 3D joint surface of the lower block is shown in Fig. 15b. The 2D joint surface profile line used in the shear test is shown in Fig. 15c. It was extracted along the shearing direction capturing the steepest slope.

Parameter values used in the particle bond model are listed in Table 5. These values were obtained by a series of uniaxial compression tests on intact granite cylinders. The physical and mechanical properties of the intact granite samples are shown in Table 6. Table 5 also shows the parameter values used in the SJCM. These values were obtained from two planar granite joints. Specifically, the BB model parameters were calibrated through the normal closure test. Shear stiffness and frictional coefficient were calibrated through the direct shear test. It should be mentioned that, in the laboratory direct shear test, the cylindrical joint specimen was placed in the centre of the shear box, and fixed with high-strength mortar. Thus, in the numerical test, an “extended” 2D joint profile model was built to reflect this loading condition. The normal stress applied was 30 MPa, which is approximately 20% of the uniaxial compressive strength of the intact granite specimen. Fig. 16 shows shear stress-shear displacement curves from numerical and laboratory direct shear tests. To a large extent, this 2D numerical direct shear test can reflect the 3D experiment shear test with respect to the shear strength, the shear displacement at peak strength, shear stiffness and the residual strength.

Fig. 17a compares shearing zones in numerical and laboratory shear tests at the shear

displacement of 5 mm. Two digital elevation models of the joint were obtained before and after the shear test by 3D laser scanning. Shearing zones were determined by comparing these two digital joint surfaces in height. Here, dark blue zones represent zones with great differences. The height difference defining the interval of contour lines is ± 0.5 mm. It can be seen from Fig. 17a that dark blue zones were located around the steepest slopes and near the joint edge, suggesting that asperities in these zones were all sheared off or even crushed. Green zones in Fig. 17a represent intact zones. The height difference defining the intact zones is ± 0.25 mm (Li, 2014). Fig. 17b shows shearing zones, i.e., cracking zones, on the 2D numerical joint model. It can be seen that the location and size of the shearing zones were similar in the numerical and experimental tests.

6 Discussion

Although a pre-shearing load has been applied before the shear test, the initial mismatch of joint surfaces, and the interspace between the shear box and the joint are still obvious, which contributes to an initial convex section on the shear stress-shear displacement curve, as shown in Fig .16. However, in the numerical simulations, rigid particles were distributed in an orderly manner on both sides of the joint plane, and shear stress was applied by moving the lateral walls bonded together with model edges. Therefore, there was no initial convex portion on the shear stress-shear displacement curve. This difference indicates that the tangent shear stiffness in the initial phase is not comparable between the experimental and numerical tests. Thus, in the present study, joint shear stiffness mentioned is the ratio of stress to displacement at the peak-stress point, named the “specific stiffness” or the “secant stiffness at the peak stress” (Karami and Stead, 2008, Li et al., 2016, Prassetyo et al., 2017). This definition emphasizes the importance of shear strength, and facilitate the comparison between numerical and experimental testing results.

In this study, shear dilation was not investigated because the normal displacements, recorded at the four corners of the upper shear box, showed nonuniform changes during

shearing. This discordance indicates that asperity degradation may cause joint rotation. It is difficult to simulate this phenomenon by 2D joint models in PFC. Further study using 3D joint models is needed in the future.

In numerical direct shear tests, stress fluctuations could be observed especially in the post-peak phase. This unstable state results from the rigid assumption of particles in PFC. In experimental tests, broken fragments are usually crushed after the peak stress, which results in a relatively smooth stress-displacement curve. Although the stress fluctuation would not affect substantively the joint shear process in our tests, its potential impacts need to be fully explored in the future.

7 Summary and conclusions

The main works and conclusions of this paper are summarised as follows:

(1). The local interlocking problem of the SBG approach was successfully solved by introducing the joint side checking method and the concept of maximum allowed closure.

(2). The periodic stress fluctuation during shearing was alleviated by the non-unified ball generation method.

(3). The BB model was embedded in the SJCM for capturing the nonlinear stress-displacement relationship of planar joints in compression.

(4). The applicability of the improved SBG approach was validated by conducting a series of direct shear and axial compression tests on planar mortar joints.

(5). The improved SBG approach also has the ability to simulate the shear behaviour of rough joints, which has been verified by numerical and experimental tests on two types of artificial saw-tooth joints and a natural granite joint.

Acknowledgements

This research is financially supported by the National Key R&D Program of China (No. 2018YFC0407002 and No. 2016YFC0600702), the Hong Kong Jockey Club and the Shenzhen Clean Energy Research Institute.

References:

Bandis, S. C., Lumsden, A. C., & Barton, N. R. (1983). Fundamentals of rock joint deformation. *International Journal of Rock Mechanics & Mining Sciences & Geomechanics Abstracts, 20*(6), 249-268.

Bahaaddini, M., Sharrock, G., & Hebblewhite, B. K. (2013). Numerical direct shear tests to model the shear behaviour of rock joints. *Computers and Geotechnics*, *51*, 101-115.

Bahaaddini, M., Hagan, P., Mitra, R., & Hebblewhite, B. K. (2016). Numerical study of the mechanical behaviour of nonpersistent jointed rock masses. *International Journal of Geomechanics, 16*(1)*,* 04015035.

Bahaaddini, M. (2017). Effect of boundary condition on the shear behaviour of rock joints in the direct shear test. *Rock Mechanics and Rock Engineering*, *50*(5), 1141-1155.

Cundall, P. A, Hart, R. D. (1992). Numerical modelling of discontinue. *International Journal of Industrial Engineering Computations, 9*(2), 101–13.

Cundall, P. A. (2000). Numerical experiments on rough joints in shear using a bonded particle model. In *Aspects of tectonic faulting* (pp. 1-9). Springer, Berlin, Heidelberg.

Deng, X. F, Chen, S. G., Zhu, J. B., Zhao, Z. Y., Zhou, Y. X., Zhao, J. (2015). UDEC-AUTODYN hybrid modeling of a large-scale underground explosion test. *Rock Mechanics and Rock Engineering*, 48, 737-747.

Duan K., Kwok C. Y, Pierce M. (2016). Discrete element method modeling of inherently anisotropic rocks under uniaxial compression loading. *International Journal for Numerical & Analytical Methods in Geomechanics, 40*(8):1150-1183.

Fakhimi, A., & Villegas, T. (2007). Application of dimensional analysis in calibration of a discrete element model for rock deformation and fracture. *Rock Mechanics & Rock Engineering, 40*(2), 193-211.

Goodman, RE. (1976). *Methods of geological engineering in discontinuous rocks*. West Pub. Co.

Hunt, S. P., Meyers, A. G., & Louchnikov, V. (2003). Modelling the Kaiser Effect and deformation rate analysis in sandstone using the discrete element method. *Computers*

& Geotechnics, 30(7), 611-621.

Ivars, D. M., Pierce, M. E., Darcel, C., Reyes-Montes, J., Potyondy, D. O., Young, R. P., & Cundall, P. A. (2011). The synthetic rock mass approach for jointed rock mass modelling. *International Journal of Rock Mechanics and Mining Sciences*, *48*(2), 219-244.

Itasca Consulting Group Inc. (2016). *PFC manual* (version 5.0). Minneapolis, USA

Kulhawy, F. H. (1975). Stress deformation properties of rock and rock discontinuities. *Engineering Geology*, *9*(4), 327-350.

Karami, A., & Stead, D. (2008). Asperity degradation and damage in the direct shear test: a hybrid FEM/DEM approach. *Rock Mechanics & Rock Engineering, 41*(2), 229-266.

Kulatilake, P. H., Shreedharan, S., Sherizadeh, T., Shu, B., Xing, Y., & He, P. (2016). Laboratory estimation of rock joint stiffness and frictional parameters. *Geotechnical and Geological Engineering*, *34*(6), 1723-1735.

Karakus, M., Liu, Y., Zhang, G., & Tang, H. (2016). A new shear strength model incorporating influence of infill materials for rock joints. *Geomechanics and Geophysics for Geo-Energy and Geo-Resources*, *2*(3), 183-193.

Leong, E., & Randolph M. (1992). A model for rock interfacial behavior. *Rock Mechanics and Rock Engineering, 25*(3), 187-206.

Li, H. (2014). *Study on basic shear behaviour of granite joints based on three-dimensional joint roughness parameters* (in Chinese). Postgraduate dissertation, Chengdu University of Technology, Chengdu, China.

Li, J. C., Li, N. N., Li, H. B., & Zhao, J. (2016). An SHPB test study on wave propagation across rock masses with different contact area ratios of joint. *International Journal of Impact Engineering, 105*, 109-116.

Li, X., Zhang, Q. B., He, L., & Zhao, J. (2016). Particle-based numerical manifold method to model dynamic fracture process in rock blasting. *International Journal of Geomechanics, 17*(5), E4016014.

Malama, B., & Kulatilake, P. H. S. W. (2003). Models for normal fracture deformation under compressive loading. *International Journal of Rock Mechanics & Mining*

Sciences, 40(6), 893-901.

Mehranpour, M. H., & Kulatilake, P. H. (2016). Comparison of six major intact rock failure criteria using a particle flow approach under true-triaxial stress condition. *Geomechanics and Geophysics for Geo-Energy and Geo-Resources*, *2*(4), 203-229.

Mehranpour, M. H., & Kulatilake, P. H. S. W. (2017). Improvements for the smooth joint contact model of the particle flow code and its applications. *Computers & Geotechnics, 87*, 163-177.

Oh, J. M. (2005). *Three-dimensional numerical modelling of excavation in rock with dilatant joints*. Doctoral dissertation, University of Illinois, Urbana, USA.

Oh, J. M., Cording, E. J., & Moon, T. (2015). A joint shear model incorporating small-scale and large-scale irregularities. *International Journal of Rock Mechanics & Mining Sciences, 76*(1), 78-87.

Plesha, M. E. (1987). Constitutive models for rock discontinuities with dilatancy and surface degradation. *International Journal for Numerical & Analytical Methods in Geomechanics, 11*(4), 345-362.

Potyondy, D. O., & Cundall, P. A. (2004). A bonded-particle model for rock. *International Journal of Rock Mechanics & Mining Sciences, 41*(8), 1329-1364.

Prassetyo, S. H., Gutierrez, M., & Barton, N. (2017). Nonlinear shear behaviour of rock joints using a linearized implementation of the Barton-Bandis model. *Journal of Rock Mechanics and Geotechnical Engineering,9*(4), 671-682.

Yang, Y., Ju, Y., Sun, Y., & Zhang, D. (2015). Numerical study of the stress field during crack growth in porous rocks. *Geomechanics and Geophysics for Geo-Energy and Geo-Resources*, *1*(3-4), 91-101.

Yin, P., & Zhao, G. F. (2016). Numerical simulation of fluid flow through deformable natural fracture network. *Geomechanics and Geophysics for Geo-Energy and Geo-Resources*, *2*(4), 343-363.

Vallejos, J. A., José Matias Salinas, Delonca, A., & Ivars, D. M. (2016). Calibration and verification of two bonded-particle models for simulation of intact rock behaviour. *International Journal of Geomechanics, 17*(4), 06016030.

Vosiniakos, K. (2007). *Physical and numerical modelling of shear behaviour of saw-toothed filled rock joint*. Doctoral dissertation, The University of Manchester, Manchester, UK.

Wang, T., Xu, D., Elsworth, D., & Zhou, W. (2016). Distinct element modeling of strength variation in jointed rock masses under uniaxial compression. *Geomechanics and Geophysics for Geo-Energy and Geo-Resources*, *2*(1), 11-24.

Zhu, J. B., Zhou, T., Liao, Z. Y., Sun, L., Li, X. B., Chen, R. (2018). Replication of internal defects and investigation of mechanical and fracture behaviours of rocks using 3D printing and 3D numerical methods with combination of X-ray computerized tomography. *International Journal of Rock Mechanics and Mining Sciences*, 106, 198–212.

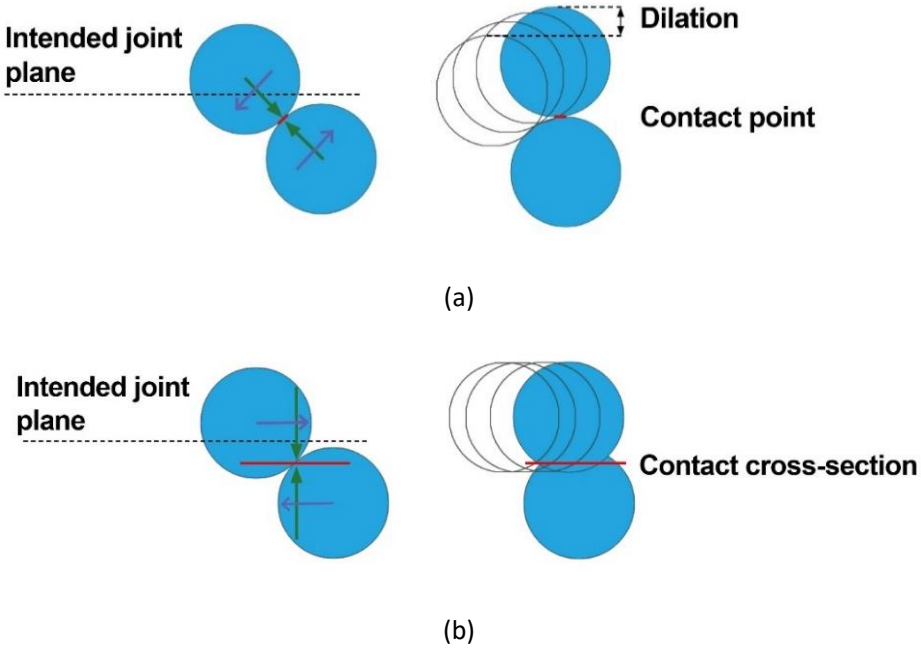

Fig. 1 Force components and particle motion: (a) under the rigid particle assumption and (b) with the SJCM. Adapted after Itasca Consulting Group Inc. (2016).

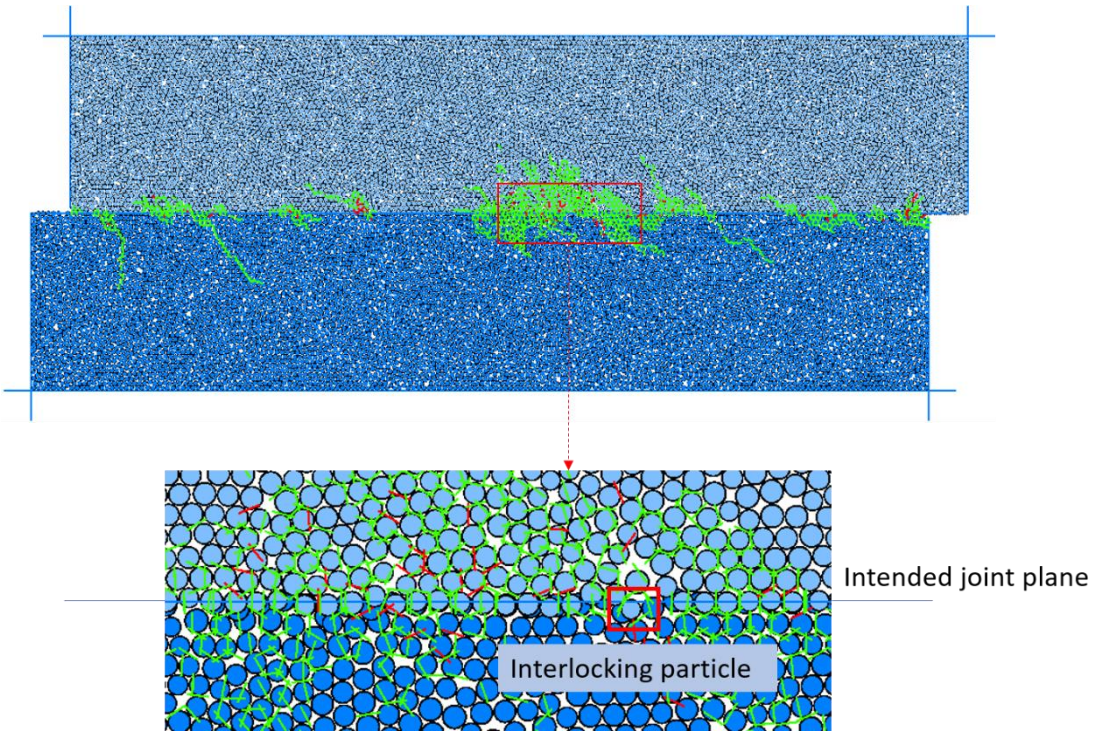

Fig. 2 Unrealistic damage on joint surfaces caused by interlocking particles in the numerical direct shear test of a planar mortar joint. The nominal size of this 2D planar joint model is 100×50 mm^2 (length×height). The radii of the particles range from 0.25 to 0.3 mm with a uniform distribution. Red represents shear cracks, and green represents tensile cracks.

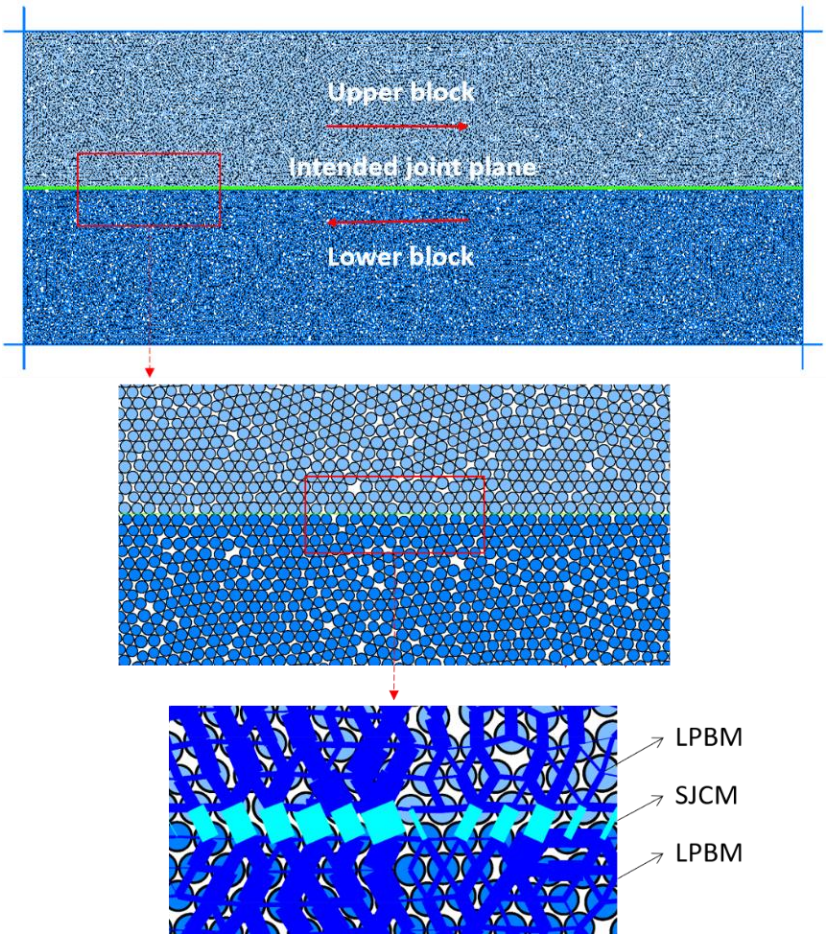

Fig. 3 The distribution of particles and contacts of a planar joints generated by the SBG approach. LPBM: linear contact bond model; SJCM: smooth joint contact model.

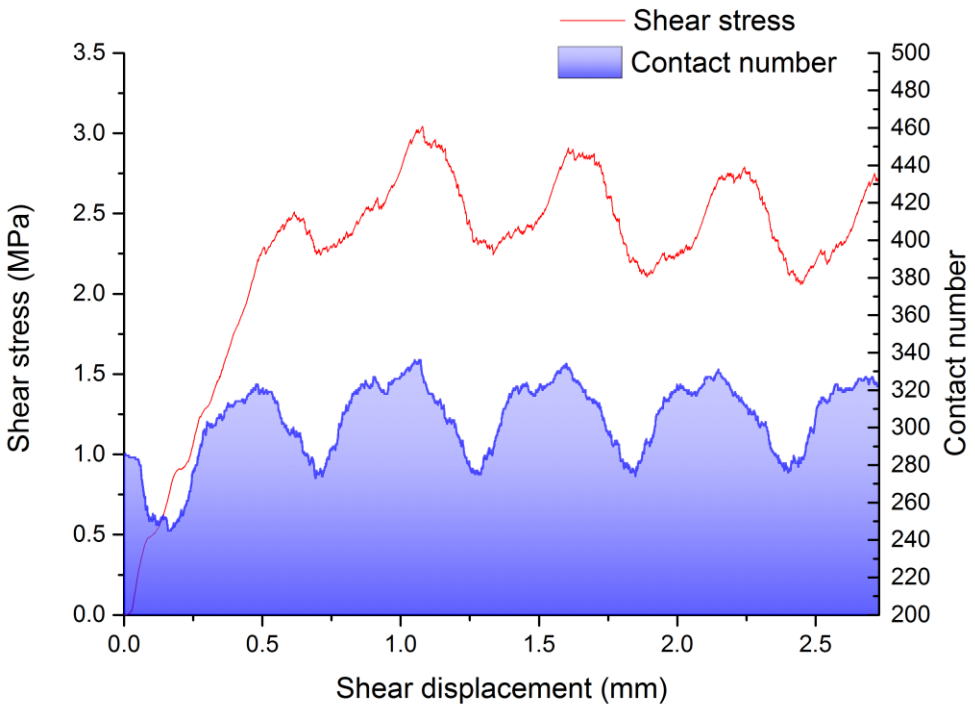

Fig. 4 The fluctuation of shear stress caused by the periodic change in contact number from the numerical direct shear test of a planar joint, generated by the SBG approach.

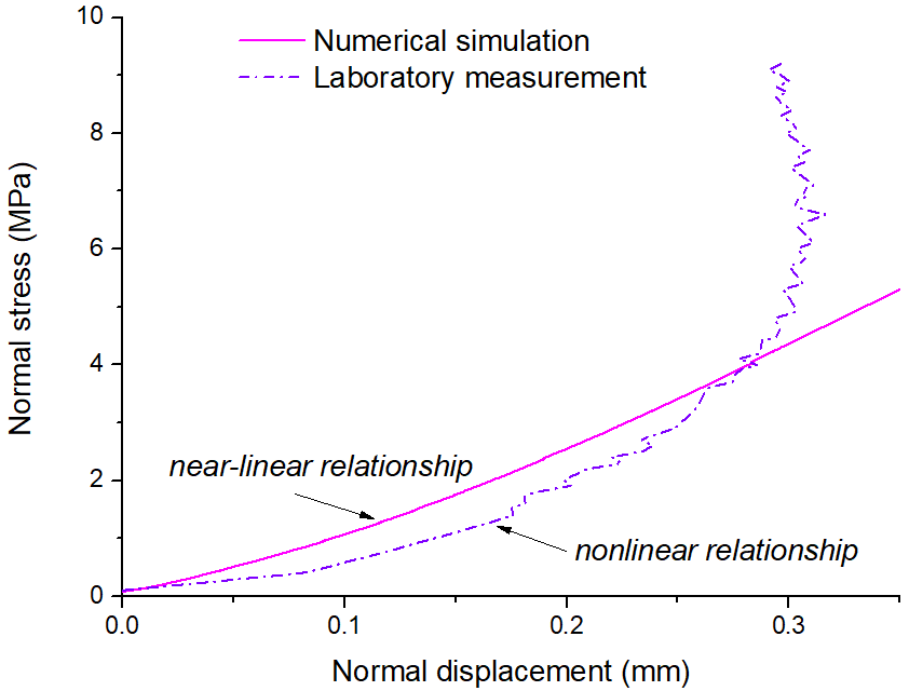

Fig. 5 Normal stress-normal displacement curves from closure tests on a planar mortar joint in both the laboratory and PFC modelling.

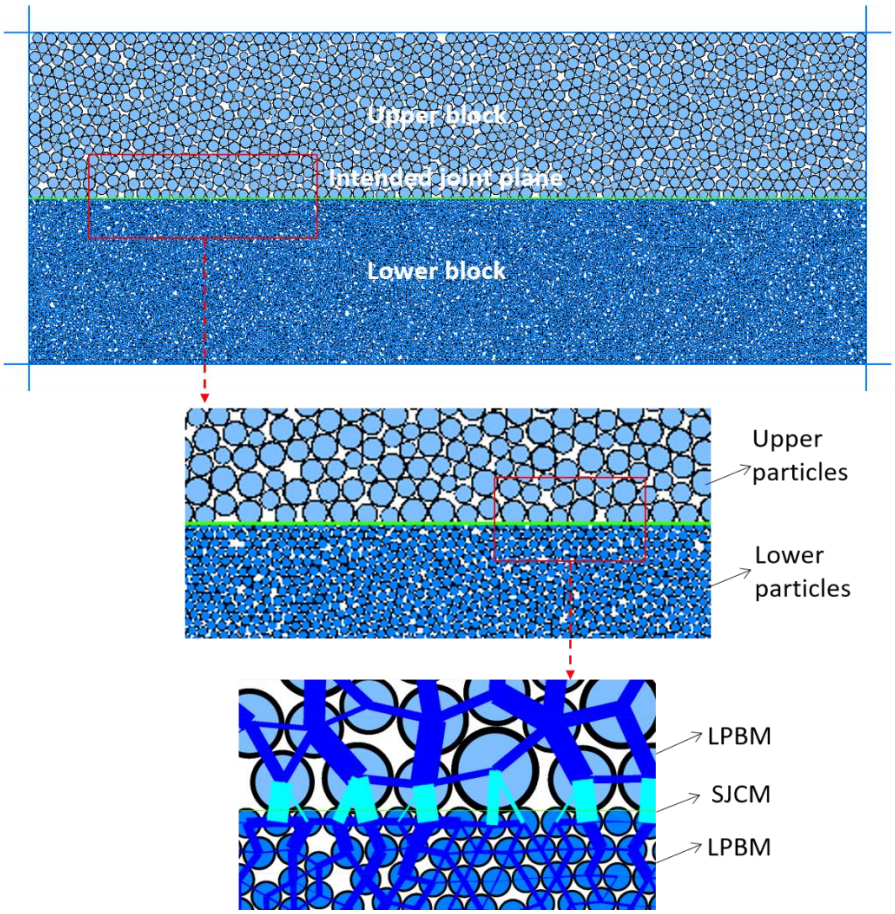

Fig. 6 The distribution of particles and contacts with the non-unified ball generation method. In this model, particle radii were selected from uniform distributions ranging from 0.25 mm to 0.3 mm in the lower block and from 0.5 mm to 0.8 mm in the upper block.

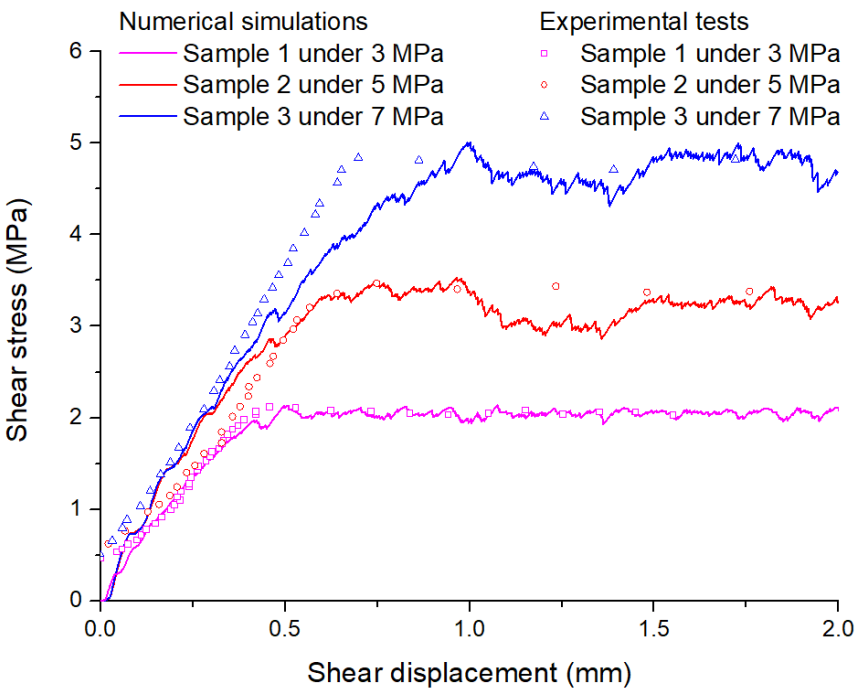

Fig. 7 Shear stress-shear displacement curves from (a) numerical and (b) experimental direct shear tests on three planar mortar joints.

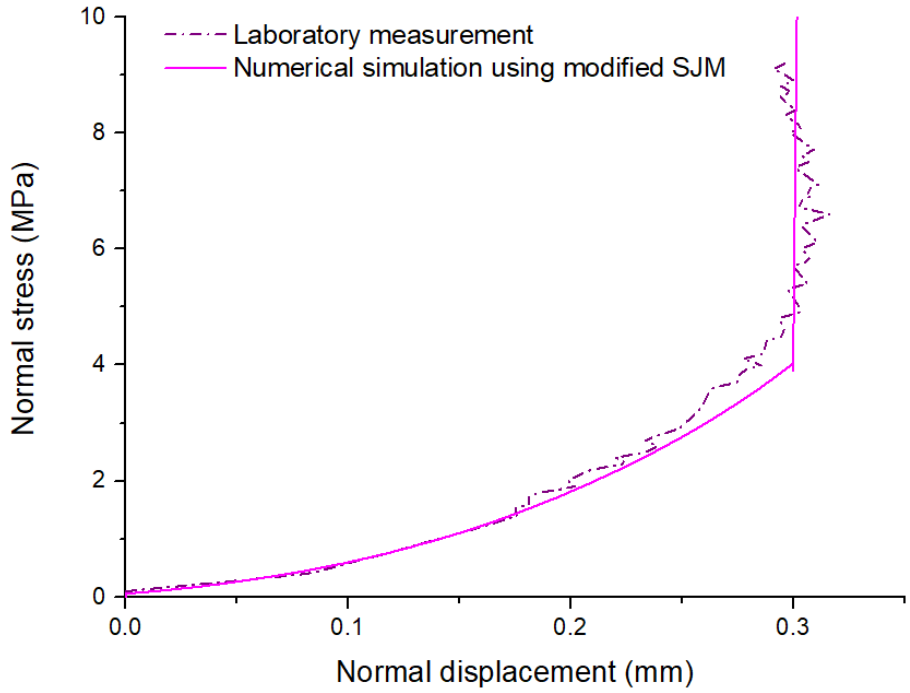

Fig. 8 Results of the numerical and experimental compression tests on a planar mortar joint. In the numerical simulation, the nonlinear closure behaviour of the joint was mathematically expressed by the BB model

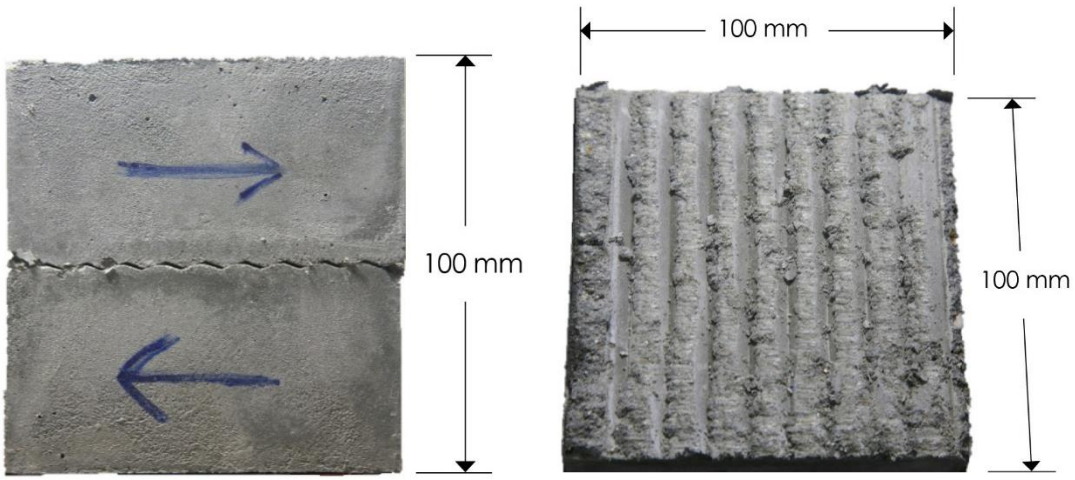

(a) (b)

Fig. 9 The artificial rough joint with regular asperities (a) before and (b) after the direct shear test. Images come from the joint specimen with 20° asperities, tested under the normal stress of 5 MPa.

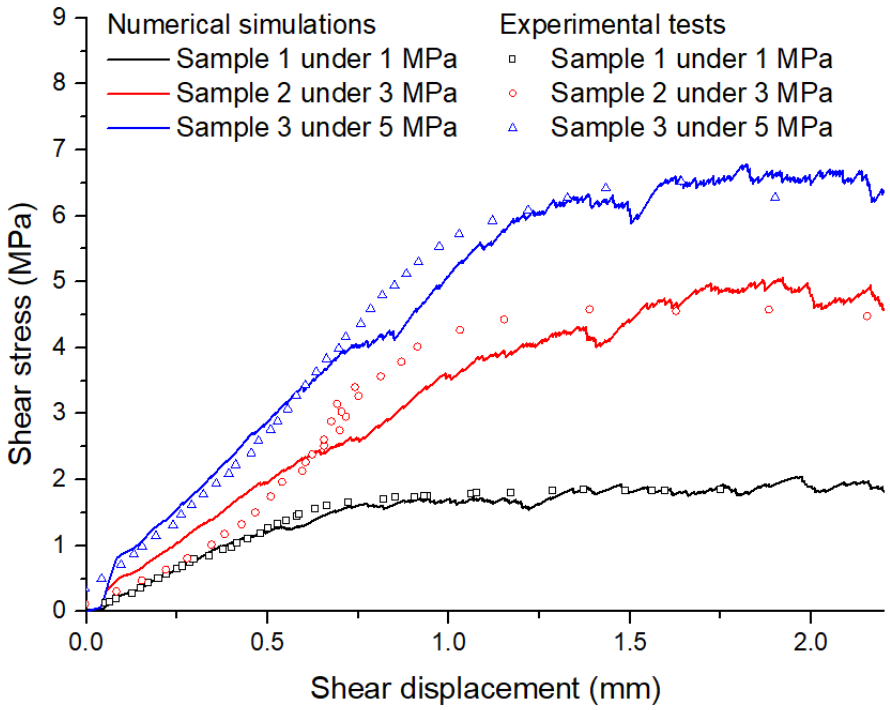

Fig. 10 Shear stress-shear displacement curves from: (a) numerical and (b) experimental direct shear tests on joints with 20° asperities.

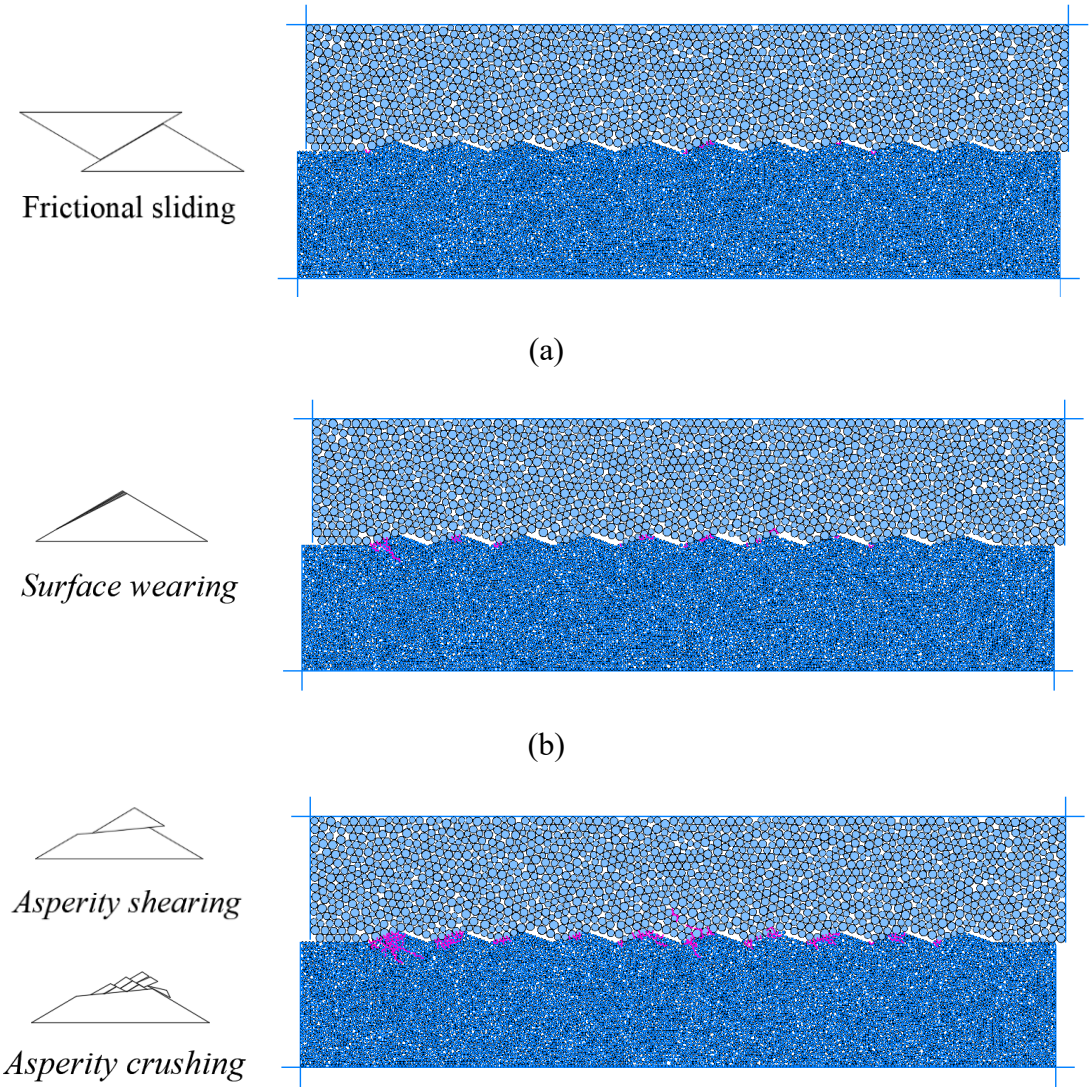

Fig. 11 Four shearing mechanisms for asperities observed in the numerical direct shear tests on saw-tooth mortar joints, where the normal stresses applied were: (a) 1 MPa; (b) 3 MPa; and (c) 5 MPa; shear displacement was 1.6 mm. Purple: cracks..

(a) (b)

Fig. 12 Joints with irregular triangular asperities: (a) before and (b) after the test (images are from the sample tested under the normal stress of 5 MPa).

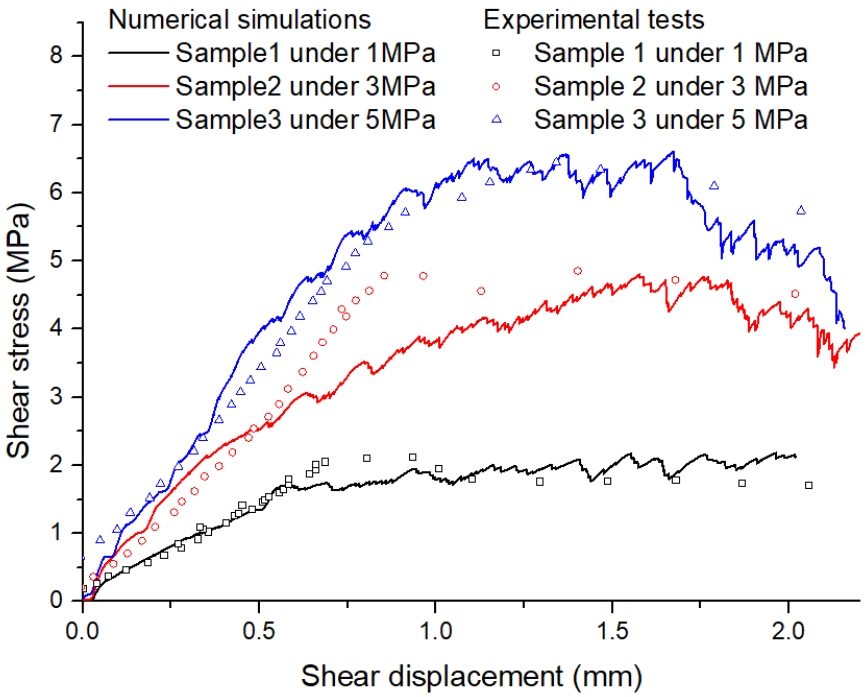

Fig. 13 Shear stress-shear displacement curves from: (a) numerical and (b) experimental direct shear tests on mortar joints with irregular asperities.

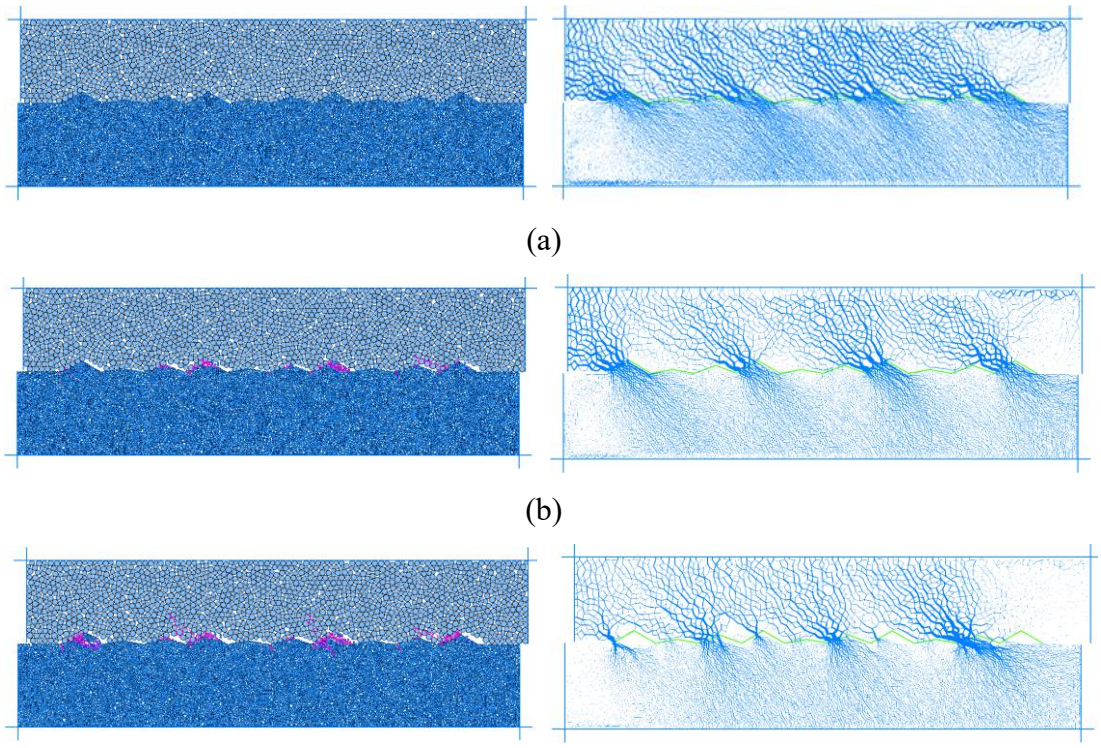

Fig. 14 Load transfer between asperities: (a) before, (b) at; and (c) after the peak shear stress during direct shear tests on artificial rough joints with irregular asperities. Left images illustrate the damage/failure process of asperities, and right figures show the change in force network, where purple and green refer to the cracks and joint surfaces, respectively. The normal stress was 3 MPa.

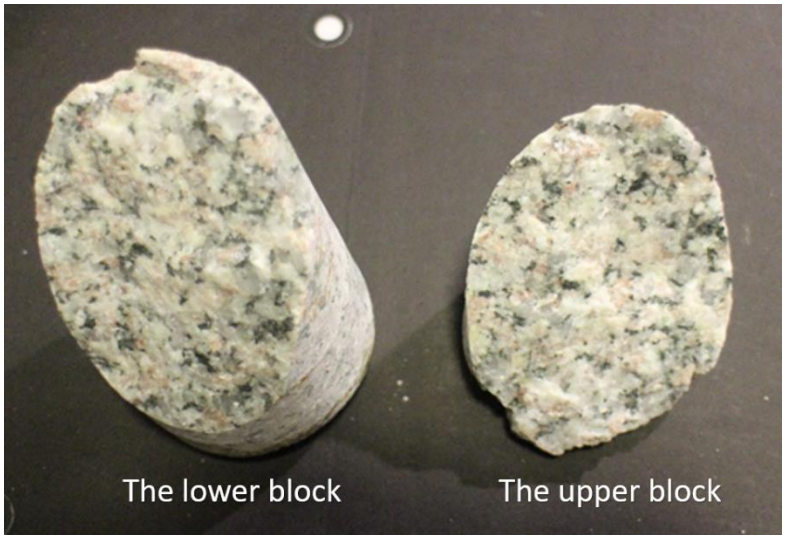

(a)

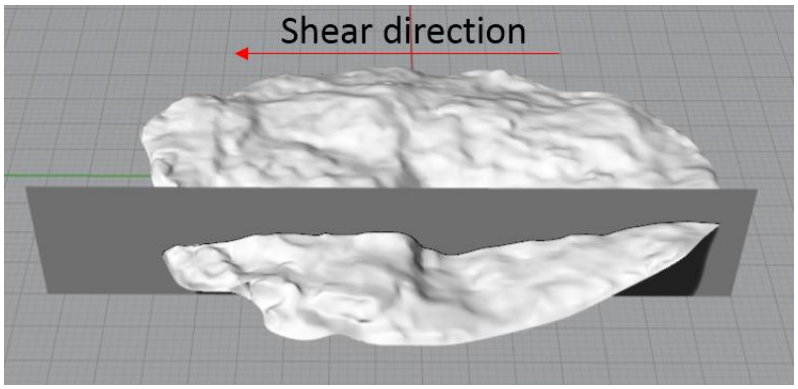

(b)

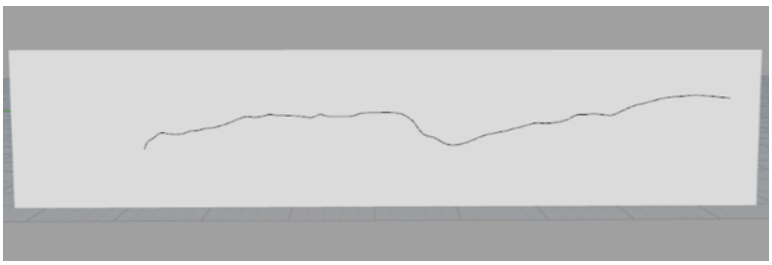

(c)

Fig. 15 (a) Natural granite joint. (b) The scanned 3D joint surface. (c) The 2D joint surface profile line used in the numerical shear test. The 2D joint profile line was extracted along the shearing direction capturing the steepest slope.

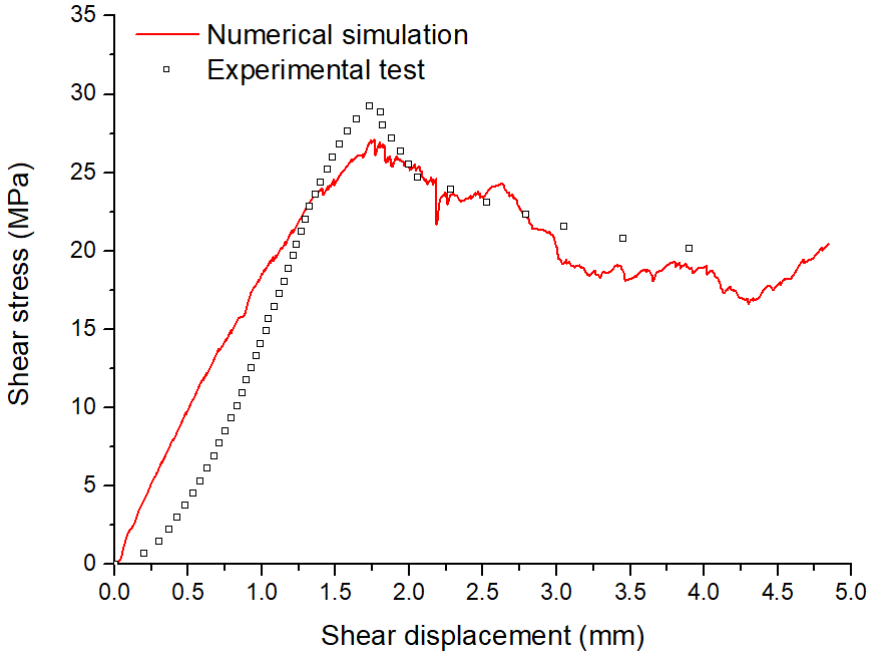

Fig. 16 Shear stress-shear displacement curves from numerical and experimental direct shear tests on a natural granite joint under the normal stress of 30 MPa.

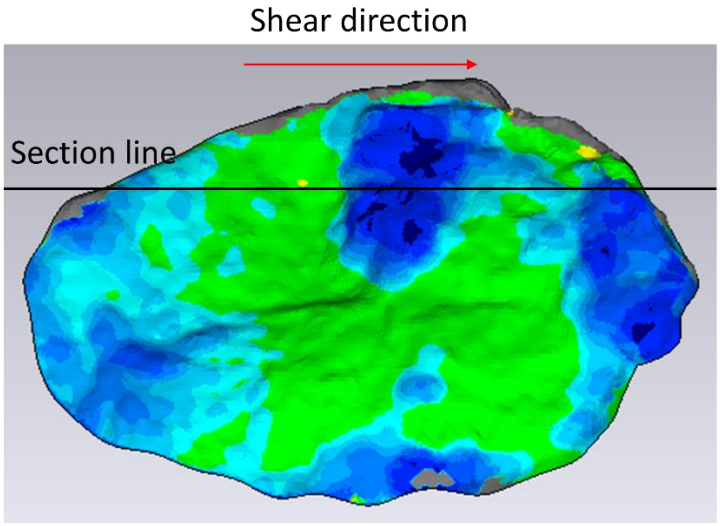

(a)

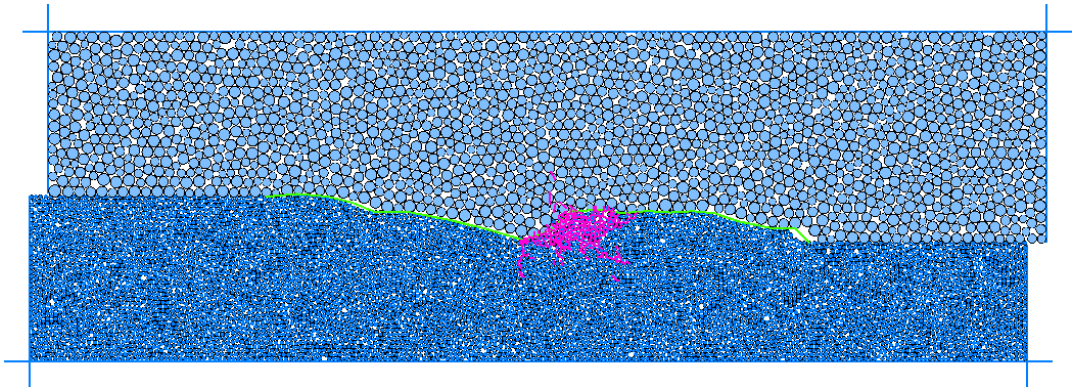

(b)

Fig. 17 Shearing zones on the granite joint: (a) 3D joint surface after the direct shear test of a natural rough joint obtained by 3D laser scanning, where shearing zones were determined by comparing the joint surfaces before and after the direct shear test (Dark blue zones represent areas with intensive shearing failure); and (b) 2D joint profile of the natural rough joint after the numerical direct shear test (purple and green refer to the cracks and the joint surface, respectively).

1

Table 1 Parameter values used in the PBM and SJCM using the SBG approach

PBM parameters	
Particle radius range (mm)	0.25-0.3
Effective modulus (GPa)	5.2
$\mathbf{k}_n/\mathbf{k}_s$	1.4
Frictional coefficient	0.6
Normal strength (MPa)	21.8
Shear strength (MPa)	21.8
SJCM parameters	
Normal stiffness (GPa/m)	11.6
Shear stiffness (GPa/m)	4.5
Frictional coefficient	0.7

PBM: particle bond model

2

Table 2 Parameter values used in the PBM and SJCM using the non-unified ball generation method

PBM parameters	*The upper block*	*The lower block*
Particle radius range (mm)	0.5-0.8	0.25-0.3
Effective modulus (GPa)	5.9	5.2
$\mathbf{k}_n/\mathbf{k}_s$	1.57	1.4
Frictional coefficient	0.6	0.6
Normal strength (MPa)	23	21.8
Shear strength (MPa)	23	21.8
SJCM parameters		
Normal stiffness (GPa/m)	21.6	
Shear stiffness (GPa/m)	8.9	
Frictional coefficient	0.7	

1

Table 3 Testing results from the numerical and experimental uniaxial compression tests on intact mortar cylinders

		UCS (MPa)	Young's modulus (GPa)	Poisson's ratio
Experimental	Average	34	7.95	0.21
Numerical	Upper block	33.9	8.19	0.19
	Lower block	34.2	8.01	0.19

2 UCS: uniaxial compressive strength

Table 4 Parameters values used in the SJCM

BB model parameters	
Initial normal stiffness k_{ini} (GPa/m)	6
Compression displacement limit δ_{lim} (mm)	0.397
Other user-defined parameters	
Compression stiffness of joint walls (GPa/m)	100
Maximum allowable closure δ_{max} (mm)	0.3
Shear stiffness (GPa/m)	0
Frictional coefficient	0.7

1

Table 5 Parameter values used in the PBM and SJCM to simulate granite joints

PBM parameters	*The upper block*	*The lower block*
Particle radius range (mm)	0.5-0.8	0.25-0.3
Effective modulus (GPa)	39.9	35.2
$\mathbf{k}_n/\mathbf{k}_s$	1.57	1.4
Frictional coefficient	0.6	0.6
Normal strength (MPa)	101.8	91.8
Shear strength (MPa)	101.8	91.8
Improved SJCM parameters		
Initial normal stiffness k_{ini} (GPa/m)	12	
Compression displacement limit δ_{lim} (mm)	0.489	
Compression stiffness of joint walls (GPa/m)	600	
Maximum allowable closure δ_{max} (mm)	0.42	
Shear stiffness (GPa/m)	12.6	
Frictional coefficient	0.8	

1

1 Table 6 Physical and mechanical properties of the granite cylinders

Density	**UCS**	**Young's modulus**	**Poisson's ratio**
2.56 g/cm^3	148 MPa	52.37 GPa	0.18

2